J|A|C|S COMMUNICATIONS

Published on Web 12/16/2009

Direct Probing of Spin State Dynamics Coupled with Electronic and Structural Modifications by Picosecond Time-Resolved XAFS

Shunsuke Nozawa,*[,†,||] Tokushi Sato,[‡] Matthieu Chollet,[‡,⊥] Kouhei Ichiyanagi,[¶,#] Ayana Tomita,[‡] Hiroshi Fujii,[§] Shin-ichi Adachi,[¶] and Shin-ya Koshihara[‡]

ERATO, Japan Science and Technology Agency, 1-1 Oho, Tsukuba, Ibaraki 305-0801, Japan, Tokyo Institute of Technology, 2-12-1 Oh-okayama, Meguro-ku, Tokyo 152-8551, Japan, High Energy Accelerator Research Organization, 1-1 Oho, Tsukuba, Ibaraki 305-0801, Japan, and Institute for Molecular Science and Okazaki Institute for Integrative Bioscience, Myodaiji, Okazaki 444-8787, Japan

Received September 12, 2009; E-mail: noz@post.kek.jp

Molecular magnetic systems such as nanomagnets and biological systems have attracted much interest in resent years.[1−5] In disordered magnetic systems, where the spin system does not have macroscopic magnetization, it is crucial to directly observe the transient spin states to aid in the understanding and controlling of the dynamic magnetic properties. In studies of ultrafast spin dynamics, pico- and femtosecond time scales are now accessible with advanced optical pump−probe measurement using two ultrafast lasers. However, it is not trivial to deconvoluting the dynamics of the spin state from transient optical signal. Although the magneto-optical effect has been applied to macroscopic magnetization,[6] it is difficult to apply in disordered magnetic systems. To overcome these difficulties, a pulsed hard X-ray has been utilized as a probe for the dynamics of the inner-atomic transitions.

At the *K*-edge of transition metals, which are typically the elements which make up magnetic systems, X-ray absorption fine structure (XAFS) spectra can be classified into three regions: pre-edge peaks, X-ray absorption near-edge structure (XANES), and extended X-ray absorption fine structure (EXAFS). These mainly contain information about the spin state, the electronic state, and molecular structure, respectively.[7] The pre-edge peaks reveal information about the spin state of the 3*d* electrons in the metal ion as the peaks are attributed to the 1*s*−3*d* quadrupole transition.[8,9] Therefore, time-resolved XAFS uniquely probes the spin dynamics. In addition to this, the electronic and molecular configurations can be tracked simultaneously for a particular excited state.[10,11] This is the greatest advantage in using hard X-rays, as electronic and molecular structural modifications can be studied in depth, provided there is a redistribution of the 3*d* electrons.

In aqueous solutions of $[Fe^{II}(phen)_3]^{2+}$, an iron atom is coordinated to six nitrogen atoms from the three phenanthroline ligands and is in the low-spin (LS) configuration in the ground state.[12] This complex exhibits a strong absorption at ∼430 nm due to a metal-to-ligand charge transfer (MLCT) to the singlet[1] MLCT state.[13,14] In the relaxation process from the singlet state to the LS ground state, spectral changes in visible region attributed to the formation of an intermediate state have been reported.[15] The intermediate state is generated within 1 ps and relaxes to the LS state with a subnanosecond lifetime. Based on the optical spectrum, the intermediate state has been assumed to be a quintet high-spin (HS) state generated as a result of the spin crossover (SC) and named as a photoexcited HS state. However, no direct evidence for the transient changes in the spin state of the 3*d* electron has been reported even though spin dynamics is the essence of the ultrafast SC phenomena. Moreover, the SC from LS to HS states is closely related to the molecular structure around the metal atom, since the spin state depends on the strength of the ligand field. Therefore, the photoinduced SC in the aqueous solution of $[Fe^{II}(phen)_3]^{2+}$ provides a model for the direct measurement of spin dynamics coupled with electronic and molecular structure modifications in disordered systems. In previous studies, the transient spin state has been derived from local modulation of the electronic state and the molecular structure.[11,16] However, in this study, the transient spin state in a disordered magnetic system has for the first time been directly studied by probing the dynamic features of the 3*d* state on a picosecond time scale. In addition, studying the transient spin state allows for a more comprehensive investigation, including variations in the electronic states and molecular structure.

The pump−probe time-resolved XAFS experiments[17] were conducted at the undulator beamline NW14A of the Photon Factory Advanced Ring (PF-AR) in Tsukuba.[18] A Ti:Sapphire femtosecond laser, synchronized with the X-ray pulse, was used as a pump source to excite the MLCT band of aqueous $[Fe^{II}(phen)_3]^{2+}$. See the Supporting Information (SI) for more details.

In a divalent iron system, the spin state in the ground state can be tuned by the steric hindrance in the ligand field. $[Fe^{II}(2\text{-}CH_3\text{-}phen)_3]^{2+}$ is an analogue of $[Fe^{II}(phen)_3]^{2+}$ which has an HS ground state[1] due to steric hindrance between the methyl groups of the ligands. In the top part of Figure 1a, Fe *K*-pre-edge peaks of $[Fe^{II}(phen)_3]^{2+}$ in an LS ground state and $[Fe^{II}(2\text{-}CH_3\text{-}phen)_3]^{2+}$ in the HS ground state are indicated by the solid and dotted lines, respectively. The features, corresponding to many-electron states, arise from the $d^{(n+1)}$ final state of the absorption process.[8,9] In the $^1A_1$ LS and $^5T_2$ HS states, the transition of an electron from an Fe 1*s* orbital to the localized Fe 3*d* orbitals produces the electron configurations shown in Figure 1b. Since the $d^{(n+1)}$ many-electron states are given by the coupling of the valence electron in these configurations, the $(t_{2g})^6$ $(e_g)^1$ configuration provides an ^2E_g state in the LS case. In the HS analogy, the $(t_{2g})^5(e_g)^2$ configuration provides a $^4T_{1g}$ state and the $(t_{2g})^4$ $(e_g)^3$ configuration gives $^4T_{1g}$ and $^4T_{2g}$ states.[8,20] To investigate the photoexcited HS state in $[Fe^{II}(phen)_3]^{2+}$, a time-resolved XAFS experiment was conducted with pulsed laser excitation at the MLCT band. In the bottom part of Figure 1a, a difference spectrum of $[Fe^{II}(phen)_3]^{2+}$ before and after the laser excitation at 50 ps is plotted as a transient difference spectrum (circles) and can be compared with the difference spectrum of the LS ground state of $[Fe^{II}(phen)_3]^{2+}$ and the HS analogue $[Fe^{II}(2\text{-}CH_3\text{-}$

† ERATO, Japan Science and Technology Agency.
|| Present address: High Energy Accelerator Research Organization, 1-1 Oho, Tsukuba, Ibaraki 305-0801, Japan.
‡ Tokyo Institute of Technology.
⊥ Present address: Advanced Photon Source, Argonne National Laboratory, Argonne, IL 60439, USA.
¶ High Energy Accelerator Research Organization.
# Present address: Graduate School of Frontier Sciences, The University of Tokyo, 5-1-5 Kashiwanoha, Kashiwa, Chiba 277-8562, Japan.
§ Institute for Molecular Science and Okazaki Institute for Integrative Bioscience.

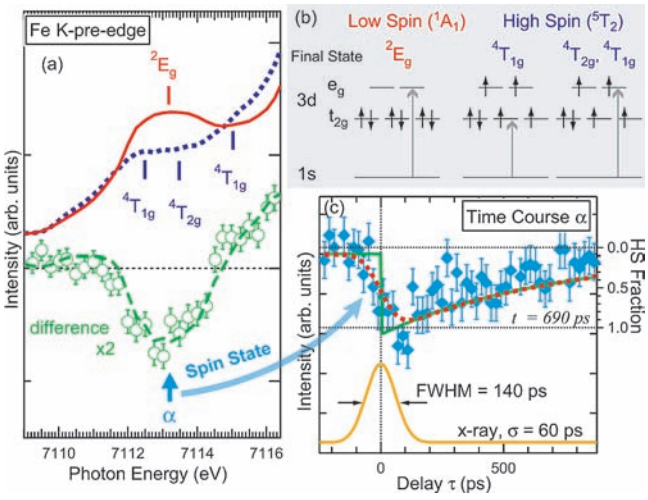

Figure 1. (a, Top) Ground state Fe *K*-pre-edge peaks of $[Fe^{II}(phen)_3]^{2+}$ (LS, solid line) and $[Fe^{II}(2\text{-}CH_3\text{-}phen)_3]^{2+}$ (HS analogue, dotted line) in aqueous solution. (a, Bottom) Pre-edge peaks of the difference between the ground states of the HS analogue and LS spectra (dashed line), and the transient difference 50 ps after the excitation of the MLCT band (○). (b) The electron configurations of the $d^{(n+1)}$ final states. (c) Time course of the intensity (◆), measured at α in difference XAFS spectra. The dotted lines represent the fitting analysis by the exponential convergence with the step function (solid line) convoluted by the X-ray pulse duration ($\sigma = 60$ ps). The right axis indicates the fraction of the photoexcited HS state.

phen)$_3$]$^{2+}$ (dashed line). In the pre-edge region, the transient difference spectrum can be scaled to the static difference spectrum which reveals a 6.7% yield of the $^5T_2$ HS states in 3*d* electrons at 50 ps after the photoexcitation. This corresponds to a population factor of 1/15. These results clearly show the first direct evidence that the photoexcited HS state in $[Fe^{II}(phen)_3]^{2+}$ takes a quintet HS configuration.

The time course of the intensity at α in the difference spectra is plotted in Figure 1c against the delay time τ between the X-ray and the laser. The photoinduced conversion from $^1A_1$ to the lowest energy excited state $^5T_2$ via the ^{1} MLCT state and other short-lived intermediate states occurs within 1 ps.[15] The conversion is approximated by a step function at $\tau = 0$ ps as the time scale is relatively short compared with the $\sigma \sim 60$ ps of the X-ray pulse duration. The lifetime of the photoexcited HS state was derived by fitting the data with an exponential function. The fitting did not seem to be unduly effected by the use of a step function to approximate the formation of the state, which was intractably convoluted with the X-ray pulse duration. The lifetime is in good agreement with the value estimated from the optical experiment.[15] Moreover, the evolution over time can be assigned to vibrational relaxations in the two-level system from the photoexcited HS state to the LS ground state (see the Transient differences of EXAFS spectra section in the SI). When the photoexcited HS state is normalized, the evolution of the intensity at α corresponds to the remaining fraction of the photoexcited HS state, as shown on the right-hand axis of Figure 1c.

Because 3*d* electrons occupy an antibonding e_g orbital in the $^5T_2$ photoexcited HS state, large modifications in the electric state and molecular structure are expected. An iron *K*-edge XAFS spectrum of the LS (solid line) and HS analogy (dashed line) ground states are shown in the top part of Figure 2a. The characteristic structures in these spectra are indicated by $A - D$ ($A' - D'$). Structures *A* (*A*′) and *B* (*B*′) in the XANES region arise from the transition of an electron from the Fe 1 *s* to the Fe 4 *p* unoccupied state, and the spectral difference in the XANES region between the LS and the HS states can be explained with a molecular orbital interpretation.[16,21,22] Whereas six of the *d* electrons occupy the t_{2g} orbital in the LS state, only two

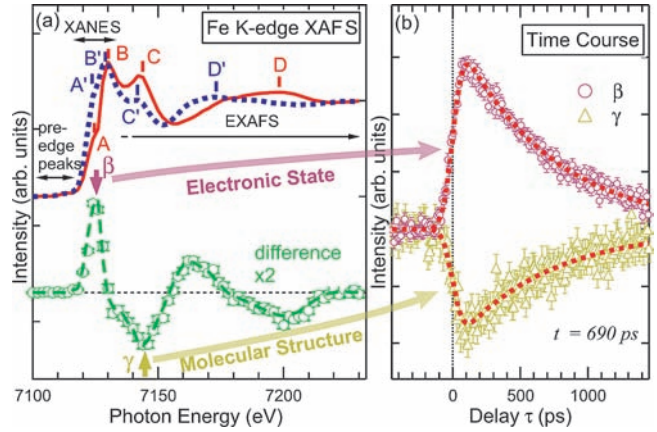

Figure 2. (a) Ground state Fe *K*-XAFS spectra in LS (solid line) and HS analogue (dotted line), and the difference between the ground state HS and LS spectra (dashed line) and the transient difference at 50 ps (○). (b) Time courses of the intensity at β and γ in the difference spectra, and the fitting curve with a decay constant of 690 ps.

d electrons occupy the σ-antibonding e_g orbital in the HS state. An increase in the bond length of Fe−N, which is associated with the spin transition, promotes a decrease in the σ-antibonding overlap between the Fe 4 *p* and N 2 *p* orbitals, and increases the Fe 4 *p* unoccupied density of states. This effect is clearly observed at the structure *A* with an increase in intensity. Moreover, σ-antibonding is stabilized from the increase in 4 *p* character resulting in an increase in the Fe−N bond lengths. As a result, the structure *B* shifts to lower energy. Structures *C* (*C*′) and *D* (*D*′) correspond to the EXAFS oscillation. The spectral changes here are caused by the modulation of the resonant effect in the multiple scattering of the photo electron when the bond length of Fe−N is increased. In this EXAFS region, the spectral changes, accompanied by an extension of the Fe−N bond length, has been accurately modeled by a full multiple scattering calculation on a simple seven-atom cluster consisting of a six-coordinated iron with nitrogen atoms.[22]

The ground state and transient difference at 50 ps are shown at the bottom of Figure 2a. Comparison of the photoexcited HS state spectra with that of the HS analog in the energy region from 7100 to 7232 eV indicates that, around the Fe atom, the local electronic state and the structures are very similar. In the difference spectra, a peak (β) in the XANES region and a dip (γ) in the EXAFS region are attributed to the local modulation of the electronic state and the molecular structure, respectively. The time courses of the intensity at β and γ are shown in Figure 2b. Fitting these data to exponential curves shows that the transient variation in structures in the XANES (β) and EXAFS (γ) regions progresses with the same time constant of 690 ps as obtained from the pre-edge region. It is clearly indicates that, on the picosecond time scale, the photoexcited HS state accompanies the coupled modifications in the spin configuration, the electronic states, and the molecular structure. In addition, in the relaxation process of the photoexcited HS state, all of the changes revert to the original LS state simultaneously.

Time-resolved EXAFS analysis gives a transient molecular structure of the photoexcited HS state. Details of the analysis can be found in the SI. The Fourier transformed EXAFS functions $k^2 \times f(k)$ of the LS, HS analog, and photoexcited HS at $\tau = 50$ ps, EXAFS spectra are shown in Figure 3a and 3b, respectively. The EXAFS spectrum of the photoexcited HS was obtained by the eq (1) in the SI. In all the Fourier transforms, a dominant contribution at ∼1.0−2.0 Å is attributed to the first nearest-neighbor (NN) in the Fe−N shell. The features appearing at ∼2.0−2.5 Å are due to the contributions from the second NN carbon atoms (Fe−C) in the phenanthroline ligands. To investigate

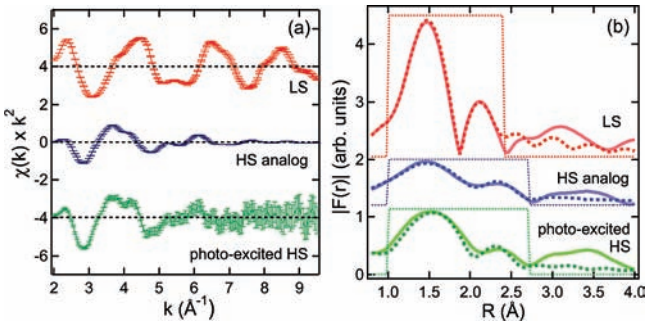

Figure 3. (a) EXAFS spectra weighted by k^2. (b) Fourier transformed EXAFS spectra (solid line). The window functions indicated by the dashed line show the *R*-range employed in the curve-fitting analysis. The dotted lines correspond to the fits of the data in *R* space, yielding the parameters listed in Table 1.

Table 1. Results of EXAFS Analysis of the Fe−N and the Fe−C Shells

Sample	Shell	*R* (Å)	σ^2 (Å^2)
LS[a]	Fe−N	1.98(1)	0.001(1)
	Fe−C	2.88(8)	0.02(2)
HS analogue[b]	Fe−N	2.15(1)	0.019(1)
	Fe−C	3.04(2)	0.014(3)
photoexcited HS[c]	Fe−N	2.15(2)	0.011(3)
	Fe−C	3.01(5)	0.02(1)

[a] $[Fe^{II}(phen)_3]^{2+}$. [b] $[Fe^{II}(2\text{-}CH_3\text{-}phen)_3]^{2+}$. [c] $[Fe^{II}(phen)_3]^{2+}$ at $\tau = 50$ ps after excited.

the molecular structures in more detail, a curve-fitting analysis using only the Fe−N and Fe−C shells was performed. The *R* range employed in the curve-fitting analysis of the LS sample was $\Delta R_{CF} \approx 1-2.4$ Å, and the HS analogue and the transient HS samples were $\Delta R_{CF} \approx 1-2.7$ Å. Fitting results are shown in Figure 3b as dotted lines and are listed in Table 1. The Fe−N distance of the LS is 1.98 ± 0.01 Å, which is a typical distance for divalent LS Fe compounds.[11,16,22] At $\tau = 50$ ps after photoexcitation, the Fe−N distance is 2.15 ± 0.02 Å, which is in good agreement with the value in the HS analogue (2.15 ± 0.01 Å) and the other divalent Fe compounds in the HS state.[16,22] Moreover, the extended Fe−N distance in the photoexcited HS state is close to the value of the excited states of $[Fe^{II}(bpy)_3]^{2+}$ (2.183 ± 0.008 Å) and $[Fe^{II}(tren(py)_3)]^{2+}$ (2.17 ± 0.03 Å) systems.[11,16] As discussed previously, the significant increase in the Fe−N bond length is consistent with the spectral change in Figure 2a. The increase in the disorder factor σ^2 from 0.001 Å^2 for the LS to 0.019 Å^2 (0.011 Å^2) for the photoexcited HS state (HS analogue) reflects the decreasing intensity and the broadening of the peaks in the Fourier transform spectra shown in Figure 3. The Fe−C shell is also expanded from 2.88 ± 0.08 Å to 3.01 ± 0.05 Å in the photoexcited HS state. This increase in bond length corresponds to the photoinduced movement of the phenanthroline ligands and matches the value in the HS analogue of 3.04 ± 0.02 Å.

In summary, the transient SC transition has been directly observed by detecting the evolution of the 1*s*−3*d* transition on the picosecond time scale. The observation of the spin dynamics provides for a comprehensive time-resolved XAFS investigation into the excited-state kinetics including the variation of electron state and molecular structure. When the material has magnetic elements, the inner atomic transitions, time-resolved XAFS process has great advantages for atom-specific dynamic investigations. In a disordered magnetic system, this experimental technique is particularly well suited to capturing ultrafast photoinduced reactions in spin crossover transitions as well as in magnetic photocatalysts,[3] nanomagnets,[4] and biological magnetic systems.[5,23] Time resolved XAFS provides precise local dynamic information around the absorption atom, as demonstrated in this study. However, time-resolved X-ray liquidography, which has achieved success in investigating the dissociation dynamics[24] and the excited state in a macromolecular system,[25] gives full structural information including solvents and solutes. A combination of these complementary experiments is helpful in understanding the overall molecular reaction dynamics.

Acknowledgment. The authors thank Hyotcherl Ihee for the use of the liquid jet system. This work was performed with the approval of the Photon Factory Program Advisory Committee (Proposal No. 2004S1-001).

Supporting Information Available: Details of experimental setup for the time-resolved XAFS, time-resolved EXAFS analysis, transient differences of EXAFS spectra, and complete ref 18. This material is available free of charge via the Internet at http://pubs.acs.org.

References

(1) Kahn, O.; Martinez, C. J. *Science* **1998**, *279*, 44–48.
(2) Gatteschi, D.; Sessoli, R. *Angew. Chem., Int. Ed.* **2003**, *42*, 268–297.
(3) Beydoun, D.; Amal, R.; Low, G. K.-C.; McEvoy, S. *J. Phys. Chem. B* **2000**, *104*, 4387–4396.
(4) Karasawa, S.; Zhou, G.; Morikawa, H.; Koga, N. *J. Am. Chem. Soc.* **2003**, *125*, 13676–13677.
(5) Sato, F.; Shiro, Y.; Sakaguchi, Y.; Suzuki, T.; Iizuka, T.; Hayashi, H. *J. Biol. Chem.* **1990**, *265*, 2004–2010.
(6) Sato, Y.; Ohkoshi, S.; Hashimoto, K. *J. Appl. Phys.* **2002**, *92*, 4834–4836.
(7) *X-Ray Absorption: Principles, Applications, Techniques of EXAFS, SEXAFS and XANES*; Koningsberger, D. C., Prins, R., Eds.; John Wiley & Sons: New York, 1988.
(8) Westre, T. E.; Kennepohl, P.; DeWitt, J. G.; Hedman, B.; Hodgson, K. O.; Solomon, E. I. *J. Am. Chem. Soc.* **1997**, *119*, 6297–6314.
(9) Vankó, G.; Neisius, T.; Molnár, G.; Renz, F.; Kárpáti, S.; Shukla, A.; de Groot, F. M. F. *Coord. Chem. Rev.* **2006**, *110*, 11647–11653.
(10) (a) Chen, L. X.; Jäger, W. J. H.; Jennings, G.; Gosztola, D. J.; Munkholm, A.; Hessler, J. P. *Science* **2001**, *292*, 262–264. (b) Bressler, C.; Saes, M.; Chergui, M.; Grolimund, D.; Abela, R.; Pattison, P. *J. Chem. Phys.* **2002**, *116*, 2955–2966. (c) Chen, L. X.; Jennings, G.; Liu, T.; Gosztola, D. J.; Hessler, J. P.; Scaltrito, D. V.; Meyer, G. J. *J. Am. Chem. Soc.* **2002**, *124*, 10861–10867. (d) Saes, M.; Bressler, C.; Abela, R.; Grolimund, D.; Johnson, S. L.; Heimann, P. A.; Chergui, M. *Phys. Rev. Lett.* **2003**, *90*, 047403(1)−047403(4). (e) Chen, L. X.; Shaw, G. B.; Novozhilova, I.; Liu, T.; Jennings, G.; Attenkofer, K.; Meyer, G. J.; Coppens, P. *J. Am. Chem. Soc.* **2003**, *125*, 7022–7034. (f) Gawelda, W.; Johnson, M.; de Groot, F. M. F.; Abela, R.; Bressler, C.; Chergui, M. *J. Am. Chem. Soc.* **2006**, *128*, 5001–5009. (g) Chen, L. X.; Zhang, X.; Wasinger, E. C.; Attenkofer, K.; Jennings, G.; Muresan, A. Z.; Lindsey, J. S. *J. Am. Chem. Soc.* **2007**, *129*, 9616–9618.
(11) (a) Gawelda, W.; Pham, V. T.; Benfatto, M.; Zaushitsyn, Y.; Kaiser, M.; Grolimund, D.; Johnson, S. L.; Abela, R.; Hauser, A.; Bressler, C.; Chergui, M. *Phys. Rev. Lett.* **2007**, *98*, 057401(1)−057401(4). (b) Bressler, C.; Milne, C.; Pham, V.-T.; ElNahhas, A.; van der Veen, R. M.; Gawelda, W.; Johnson, S.; Beaud, P.; Grolimund, D.; Kaiser, M.; Borca, C. N.; Ingold, G.; Abela, R.; Chergui, M. *Science* **2009**, *323*, 489–492. (c) Gawelda, W.; Pham, V.-T.; van der Veen, R. M.; Grolimund, D.; Abela, R.; Chergui, M.; Bressle, C. *J. Chem. Phys.* **2009**, *130*, 124520(1)124520(9) .
(12) *Spin Crossover in Transition Metal Compounds I−III*; Gütlich, P., Goodwin, H. A., Eds.; Springer: Berlin, 2004.
(13) Bosnich, B. *Inorg. Chem.* **1968**, *7*, 2379–2386.
(14) Jørgensen, C. K. *Acta. Chem. Scan.* **1957**, *11*, 166–178.
(15) McCusker, J. K.; Walda, K. N.; Dunn, R. C.; Simon, J. D.; Magde, D.; Hendrickson, D. N. *J. Am. Chem. Soc.* **1993**, *115*, 298–307.
(16) Khalil, M.; Marcus, M. A.; Smeigh, A. L.; McCusker, J. K.; Chong, H. H. W.; Schoenlein, R. W. *J. Phys. Chem. A* **2006**, *110*, 38–44.
(17) (a) Saes, M.; van Mourik, F.; Gawelda, W.; Kaiser, M.; Chergui, M.; Bressler, C.; Grolimund, D.; Abela, R. *Rev. Sci. Instrum.* **2004**, *75*, 24–30. (b) Chen, L. X. *Angew. Chem., Int. Ed.* **2004**, *43*, 2886–2905. (c) Bressler, C.; Chergui, M. *Chem. Rev.* **2004**, *104*, 1781–1812. (d) Chen, L. X. *Annu. Rev. Phys. Chem.* **2005**, *56*, 221–254.
(18) Nozawa, S.; et al. *J. Synchrotron Radiat.* **2007**, *14*, 313–319.
(19) Irving, H.; Cabell, M. J.; Mellor, D. H. *J. Chem. Soc.* **1953**, 3417–3426.
(20) Sugano, S.; Tanabe, Y.; Kamimura, H. *Multiplets of Transition Metal Ions in Crystals*; Academic Press: New York, 1970.
(21) Griffith, J. S. *The Theory of Transition Metal Ions*; Cambridge University Press: Cambridge, 1961.
(22) Briois, V.; Saintcavit, P.; Long, G. J.; Grandjean, F. *Inorg. Chem.* **2001**, *40*, 912–918.
(23) Orii, Y.; Webster, D. A. *J. Biol. Chem.* **1986**, *261*, 3544–3547.
(24) Ihee, H.; Lorenc, M.; Kim, T. K.; Kong, Q. Y.; Cammarata, M.; Lee, J. H.; Bratos, S.; Wulff, M. *Science* **2005**, *309*, 1223–1227.
(25) Cammarata, M.; Levantino, M.; Schotte, F.; Anfinrud, P. A.; Ewald, F.; Choi, J.; Cupane, A.; Wulff, M.; Ihee, H. *Nat. Methods* **2008**, *5*, 881–886.

JA907460B